Hindawi
Advances in Polymer Technology
Volume 2022, Article ID 7377895, 24 pages
https://doi.org/10.1155/2022/7377895

Research Article

The Effect of Starch and Magnetite on the Physicochemical Properties of Polyurethane Composites for Hyperthermia Treatment

Natalia Paprota, Piotr Szatkowski, Monika Szlachta, Wojciech Piekarczyk, and Kinga Pielichowska

AGH University of Science and Technology, Faculty of Materials Science and Ceramics, Department of Biomaterials and Composites, Al. Mickiewicza 30, 30-059 Kraków, Poland

Correspondence should be addressed to Kinga Pielichowska; kingapie@agh.edu.pl

Received 18 September 2021; Revised 24 January 2022; Accepted 24 February 2022; Published 6 April 2022

Academic Editor: Kai Guo

In this study, modified polyurethanes (PUs) with starch and magnetite were synthesized in the form of scaffolds for potential applications in orthopedics. Polyurethanes were synthesized using a one-step method. PU synthesis was carried out using poly(ε-caprolactone) 2000 as soft segments and 4,4′-methylenediphenyl diisocyanate (MDI). Various molar ratios of starch and 1,5-pentanediol (PDO) as crosslinker/chain extender were applied, and the effects of incorporating different amounts of magnetite, as well as the role of PDO to starch ratio, were studied. The use of the additive in the form of magnetic particles was to feature the polyurethane materials for use in hyperthermia. The prepared polyurethanes were investigated using Fourier transform infrared spectroscopy (FTIR), differential scanning calorimetry (DSC), thermogravimetry (TG), and dynamic mechanical analysis (DMA) methods. Scanning electron microscopy (SEM)/energy-dispersive X-ray spectroscopy (EDX) analysis and preliminary bioactivity assessment were also performed. The addition of magnetic particles did not cause significant changes in the properties of the obtained materials compared to starch. The tested materials have the potential to be used to fill or replace bone defects in orthopedics, where they can undergo hyperthermia treatment.

1. Introduction

Despite the significant development of medicine in recent years, it is still difficult to develop the appropriate techniques and materials that would enable the regeneration of bone tissue of patients with orthopedic injuries, cancer, or other bone diseases. Despite the high efficiency of autogenous or allogeneic transplants, numerous disadvantages limit their common use. This leads to the intensive development of bone loss reconstruction materials [1–4].

One of the basic and most popular polyurethane applications in medicine is implants and prostheses. The feature that distinguishes the materials used for implants from other biomaterials is their biostability. In the case of long-term implants, materials that are resistant to degradation or adequately protected against degradation should be used. Aromatic diisocyanates used for the synthesis of polyurethanes have a significant impact on their degradation. Moreover, resistance to hydrolysis, and thus the biodegradation rate, can be increased by increasing the content of hard segments in polyurethanes. Such an implant can fulfill its tasks for a long time, and it will not be necessary to replace it. This group includes materials used as breast implants or blood vessel prostheses [5–8].

Over the last few years, many materials obtained from renewable resources were used to modify synthetic polymers and fabric then innovative materials with improved properties. One of the most widely used polysaccharides is starch,

Table 1: Composition of PU/starch/magnetite samples.

Sample code	MDI (mole)	PCL (mole)	PDO (mole)	PDO: starch/mass ratio	Magnetite (mass%)
PU_0S_0M	2	1	1	1 : 0	—
PU_25S_0M	2	1	1	0.75 : 0.25	—
PU_50S_0M	2	1	1	0.5 : 0.5	—
PU_75S_0M	2	1	1	0.25 : 0.75	—
PU_100S_0M	2	1	1	0 : 1	—
PU_0S_1M	2	1	1	1 : 0	1
PU_25S_1M	2	1	1	0.75 : 0.25	1
PU_50S_1M	2	1	1	0.5 : 0.5	1
PU_75S_1M	2	1	1	0.25 : 0.75	1
PU_100S_1M	2	1	1	0 : 1	1
PU_0S_0.5 M	2	1	1	1 : 0	0.5
PU_100S_0.5 M	2	1	1	0 : 1	0.5

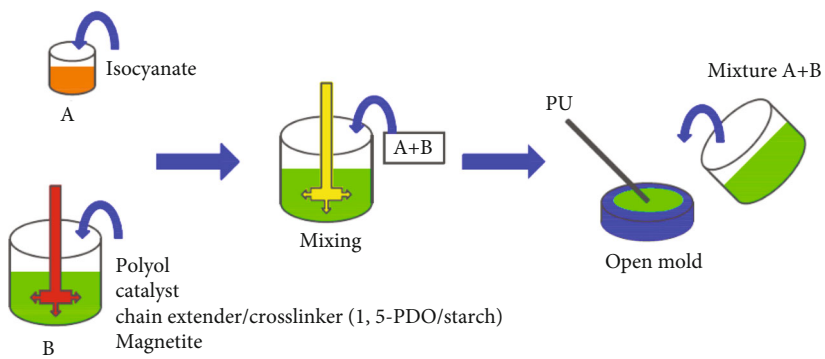

Figure 1: Scheme of sample preparation.

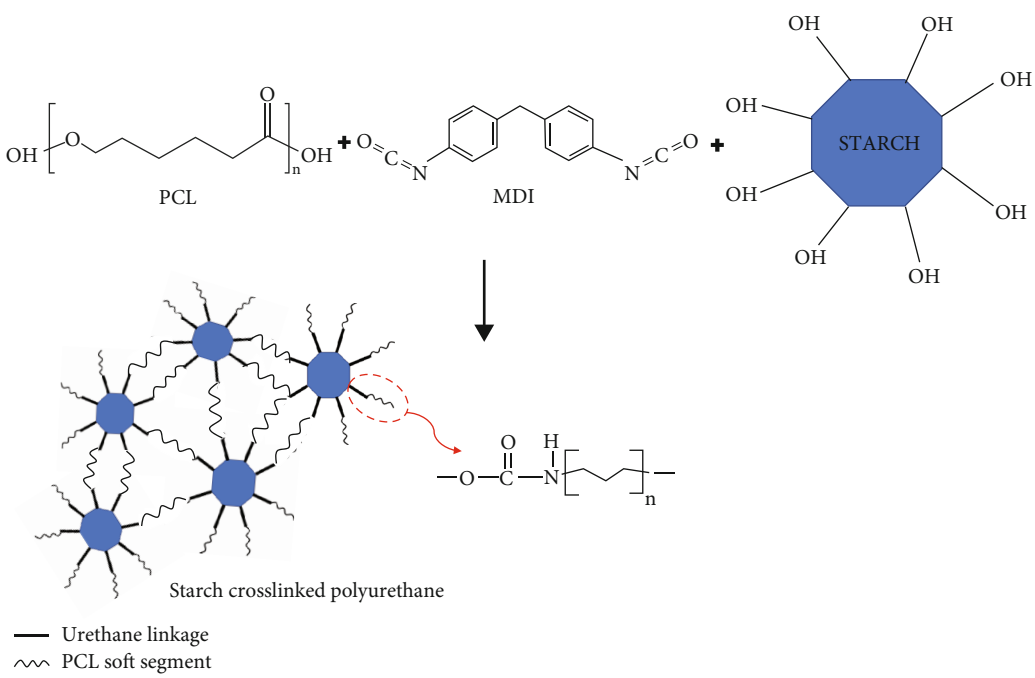

Figure 2: Reaction scheme of the formation of PU and the crosslinking by starch.

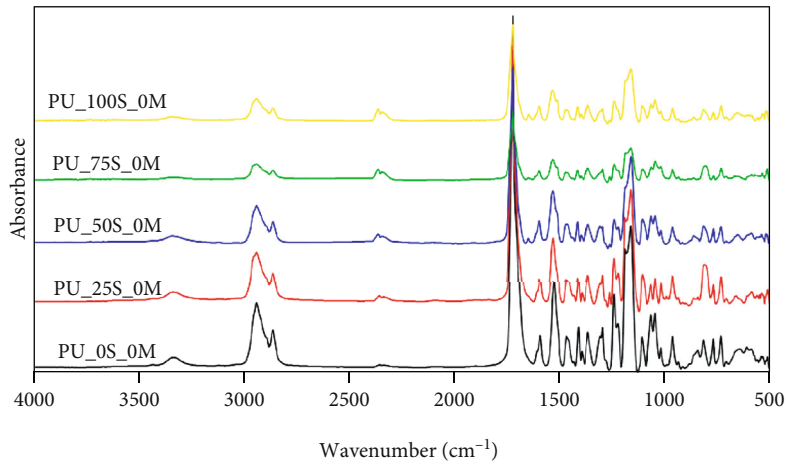

(a)

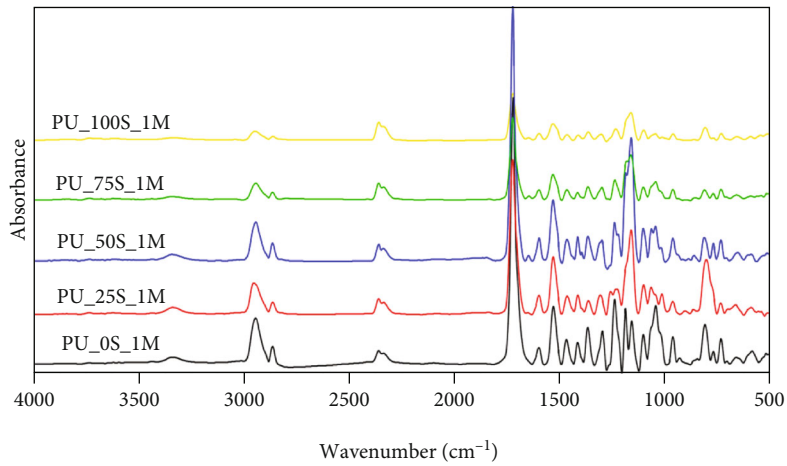

(b)

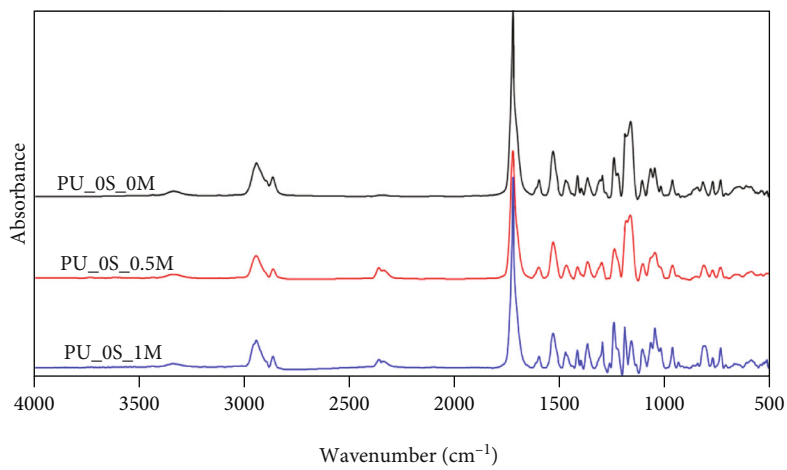

(c)

Figure 3: Continued.

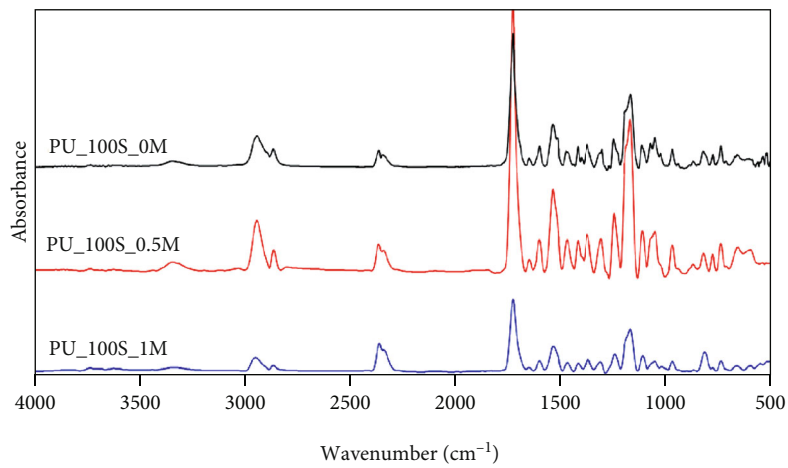

(d)

Figure 3: FTIR spectra of PU materials crosslinked using (a, b) starch and/or modified with (c, d) magnetite.

which is biodegradable, widely available, and can be chemically modified into a variety of macromolecular structures with interesting properties and applications. It is noteworthy that starch is a versatile modifier that can be used in the industrial sector not only to reduce costs but also to improve the biodegradability of synthesized materials [9, 10].

Promising results on the use of polyurethanes and polyurethane-saccharide composites have resulted in great interest in conducting further research on these materials. For example, Bil et al. [11] obtained polyurethanes containing 22–70 wt.% hard segments for bone tissue engineering applications. Poly(ε-caprolactone) diol, cycloaliphatic diisocyanate 4,4′-methylenebis(cyclohexyl isocyanate), and ethylene glycol as chain extender were used to synthesize aliphatic poly(ester-urethanes). The biocompatibility results suggested that the proliferation of human bone-derived cells (HBDCs) cultured in vitro improved with increasing hard segment content, while the osteogenic potential of HBDC decreased with increasing hard segment content. Using air-driven 3D printing technology, Ma et al. [12] obtained biodegradable polyurethane-urea (P-PUU) scaffolds based on piperazine with a gradient of its content. In vitro and in vivo biological results suggested that 3D printed P-PUU scaffolds exhibit remarkable biocompatibility and osteoconductivity, facilitating new bone formation. Barikani et al. [13] obtained biodegradable polyurethane elastomers as a result of the synthesis of poly(ε-caprolactone) (PCL) and isophorone diisocyanate (IPDI), extended by a different mass ratio of chitosan and 1,4-butanediol (BDO). As a result of the inclusion of chitosan into the polyurethane skeleton, the thermal stability was improved. The research also showed that with an increase in the chitosan content in the polyurethane backbone, the hydrophilicity decreased and the crystallinity increased.

Magnetic particles with nanometric and micrometric sizes are increasingly used in biomedical and medical applications. They can be used in special medical techniques due to their specific properties. The most important features of the particles used in medicine are nontoxicity, biocompatibility, injectability, and high accumulation in the target tissue [14, 15]. Hyperthermia is a form of therapy, widely used in the treatment of cancer, which consists of increasing the temperature of the tissues. This treatment is aimed at destroying cancer cells. However, in such a situation, there is a problem in the form of uneven heating of cancer cells. As a possible solution, magnetic particles can be introduced into the body near the tumor, which causes only a local increase in temperature. Then, under the influence of the alternating magnetic field, the orientation of the magnetic domains of the particles changes, and the resulting energy is converted into thermal energy and transferred to nearby tissues, which is manifested by a local increase in temperature. This process primarily destroys cancer cells that are less resistant to temperature (they die at temperatures above 43°C), while healthy cells can survive at higher temperatures. It is noteworthy that oxides are most often used in hyperthermia [16–18].

In recent years, PU/Fe_3O_4 composites have received considerable scientific interest. Chalid et al. obtained and characterized shape-memory PU/Fe_3O_4 nanocomposites. It was stated that well-dispersed Fe_3O_4 nanoparticles have good adhesion to the polyurethane matrix. This fact may influence the enhancement of the magnetic and mechanical properties of composite materials [19]. Zou et al. studied properties of the shape-memory nanocomposite films which were manufactured using thermoplastic PUs and oleic acid-(OA-) coated Fe_3O_4 nanoparticles by solution mixing followed by solvent casting. The purpose of applying an oleic acid layer to the surface of the nanoparticles was to prevent their agglomeration. It has been found that the recovery time of nanocomposite films in the magnetic field decreased with increasing nanoparticle content [20]. In our research, the key novelty was achieved by combining crosslinking effects induced by starch with the effects caused by the presence of magnetic particles. The use of starch in the crosslinking process improves the thermal properties of the obtained materials, while the addition of magnetite should provide functional magnetic properties.

Table 2: Interpretation of the FTIR spectra of PU materials crosslinked with starch and/or modified with magnetite.

PU_0S_0M	PU_25S_0M	PU_50S_0M	PU_75S_0M	PU_100S_0M	PU_0S_1M	PU_25S_1M	PU_50S_1M	PU_75S_1M	PU_100S_1M	PU_0S_0.5M	PU_100S_0.5M	
3343	3340	3344	3340	3348	3341	3340	3344	3344	3341	3340	3344	N-H stretching
2944	2944	2944	2944	2944	2945	2953	2944	2944	2948	2945	2944	CH_2 asymmetric stretching
2866	2866	2866	2864	2866	2864	2864	2864	2864	2862	2864	2864	CH_2 symmetric stretching
1723	1723	1723	1722	1723	1722	1725	1724	1723	1724	1723	1724	C=O stretching
1531	1531	1532	1532	1533	1531	1531	1532	1532	1532	1531	1533	N-H deformation
1414	1416	1414	1414	1414	1418	1414	1416	1416	1414	1416	1414	C-N stretching
1366	1366	1366	1366	1366	1366	1364	1366	1365	1364	1365	1365	CH_3 bending
1107	1105	1105	1105	1105	1103	1101	1103	1103	1101	1103	1103	C-O asymmetric stretching
1060	1046	1049	1040	1045	1043	1065	1044	1044	1045	1044	1045	C-O symmetric stretching
—	—	—	—	—	586	590	590	592	592	586	592	Vibrations of the Fe-O functional group

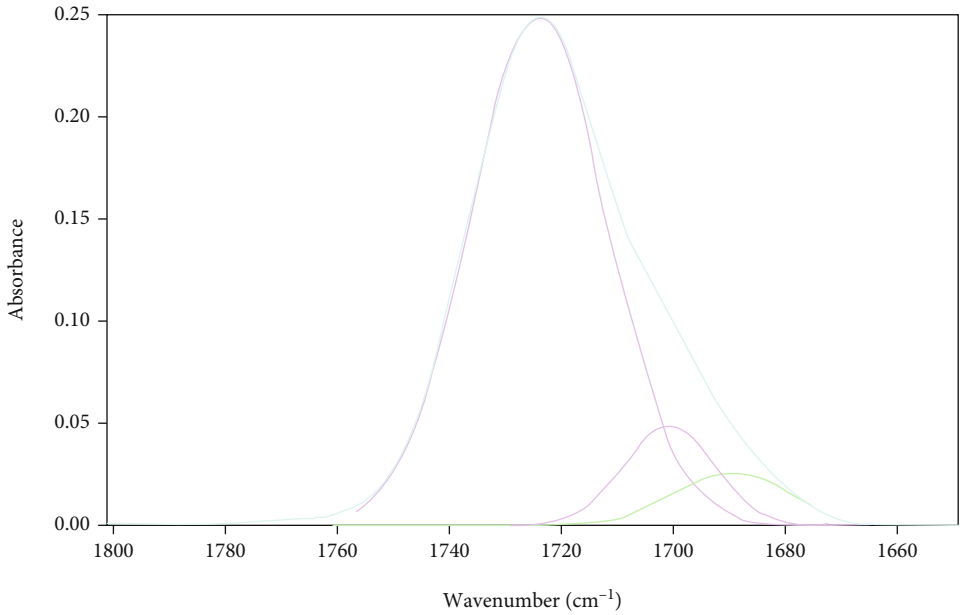

Figure 4: An exemplary result of the deconvolution of the IR C=O absorption band for PU_25S_1M.

In this study, polyurethane scaffolds containing magnetic particles were obtained and tested. This modification is aimed at expanding the use of orthopedic PU materials for the treatment of hyperthermia.

2. Experimental Part

2.1. Materials and Synthesis. PCL diol with an average molar mass of 2000, 4,4′-methylenediphenyl diisocyanate (MDI), dibutyltin dilaurate (DBTDL), and iron oxide (II, III) with diameter < 5 μm were supplied by Sigma-Aldrich. 1,5-Pentanediol (PDO) was purchased from Merck KGaA. The starch was provided by Chempur. All reagents were used as received. PCL diol, starch, and iron oxide were dried under a vacuum.

Polyurethanes were produced using a one-step method. First, the polyol masterbatch was prepared; the molten PCL and the optional modifiers (starch and/or magnetite) in appropriate amounts were placed in a plastic container and mixed using an ultrasonic homogenizer. Next, PDO and the catalyst (DBTDL) were added to the polyol masterbatch, and finally, melted MDI was introduced. The reaction mixture was mixed with a glass rod and poured into the previously prepared mold, where the polymerization process took place. The materials in the molds were placed in a vacuum oven at 37°C. The composition of the samples is presented in Table 1, and the scheme of sample preparation is displayed in Figure 1. Figure 2 exhibits the reaction scheme of the formation of PU and the crosslinking by the starch.

2.2. Techniques. Thermogravimetric analysis (TGA) was performed using the TA Instruments TGA 550 Discovery thermobalance. Samples of ca. 6-9 mg were placed in open platinum crucibles. The measurement was carried out in the 35–600°C temperature range, at a heating rate of 10°C/min under a nitrogen atmosphere. Based on the TG curves, the mass loss temperatures of 1%, 2%, 3%, 10%, and 50% and T_{DTGmax} were determined.

Table 3: Phase separation results of PU/starch/magnetite composites.

Sample code	R	DPS
PU_0S_0M	0.571	0.364
PU_25S_0M	0.115	0.103
PU_50S_0M	0.253	0.202
PU_75S_0M	0.332	0.294
PU_100S_0M	0.266	0.210
PU_0S_1M	0.396	0.284
PU_25S_1M	0.125	0.111
PU_50S_1M	0.199	0.166
PU_75S_1M	0.243	0.195
PU_100S_1M	0.358	0.264
PU_0S_0.5M	0.568	0.362
PU_100S_0.5M	0.990	0.497

Differential scanning calorimetry (DSC) analysis was performed using Mettler Toledo DSC 1. Samples (ca. 4–6 mg) were placed in closed perforated aluminum crucibles. For each sample, the measurements ran in the heating➔cooling➔heating cycle in the -70–210°C temperature range. The heating rate was 10°C/min, and the measurement was carried out under a nitrogen atmosphere.

Dynamic mechanical analysis (DMA) tests were performed on a TA Instruments DMA Discovery 850 analyzer. Measurements were carried out on cylindrical samples with a diameter of 12 mm and a height of 2–4 mm. The samples were compressed with a force of 4 or 6 N, with a frequency

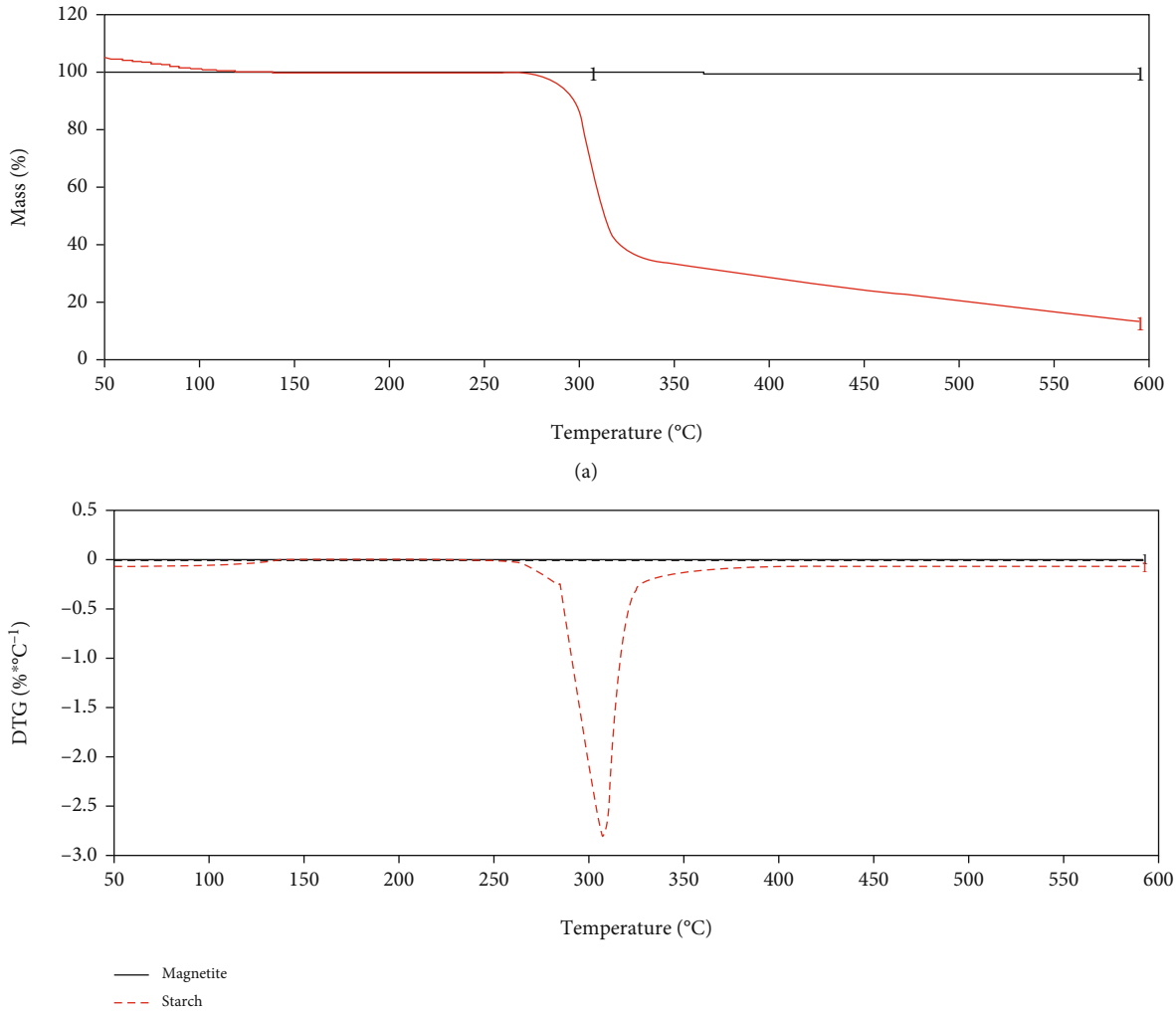

Figure 5: TG and DTG curves of pure starch and magnetite.

of 10 Hz and an amplitude of 20 μm in the temperature range -70–90°C.

Infrared (IR) experiments were performed using the Bruker Tensor 27 IR device with an ATR attachment. The samples were scanned 64 times in the spectrum range of 4000 to 500 cm^{-1} with a resolution of 2 cm^{-1}.

A scanning electron microscope (Nova NanoSEM 200, FEI, USA) equipped with an energy-dispersive X-ray analyzer (EDAX) was used to analyze the morphology of the materials obtained. Before measurement, the prepared samples were placed on the holders and coated with carbon.

Preliminary bioactivity evaluation was performed using the Kokubo method [21]. The samples were incubated in simulated body fluid (SBF) at a temperature of 37°C for 26 days. During the incubation period, the SBF was changed every 4–5 days. The samples were then washed with distilled water, dried, and subjected to microscopic analysis (SEM) to observe apatite formation on their surface.

The velocity of propagation of ultrasonic longitudinal waves was measured with the CT-3 material tester (unipan-ultrasonics), along the diameter of the samples with dimensions of approx. 17.5 mm. Measurements were made using the transition method with two heads (transmitting and receiving) with a frequency $f = 1$ MHz. The insulating tape was used as a coupling medium between the heads and the test sample. In each series of measurements, four independent measurements were made to measure the transit time of the longitudinal ultrasonic wave, and then, the average speed values and standard deviations were calculated.

3. Results and Discussion

FTIR spectra are presented in Figure 3, and the data are collected in Table 2.

Analysis of the FTIR spectra confirmed the chemical structure of the obtained polyurethanes. The lack of a band corresponding to C≡N valence vibrations (2250 cm^{-1}) proves the complete reaction of the isocyanate groups in the polyurethane synthesis reaction. All spectra show PU

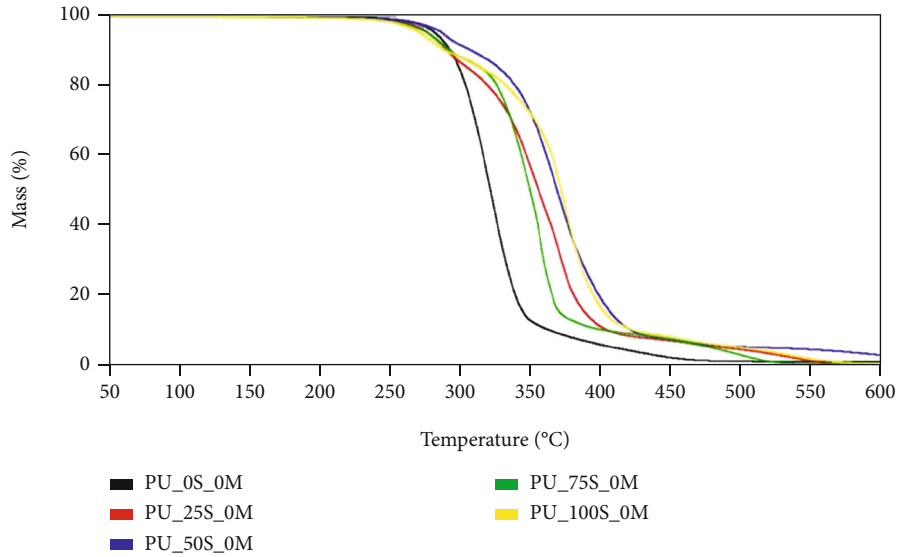

(a)

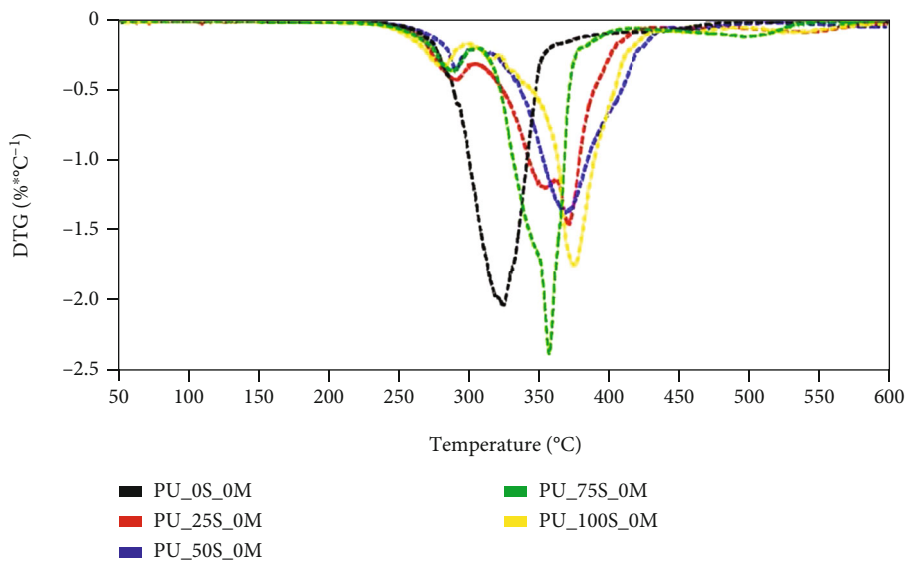

(b)

Figure 6: Continued.

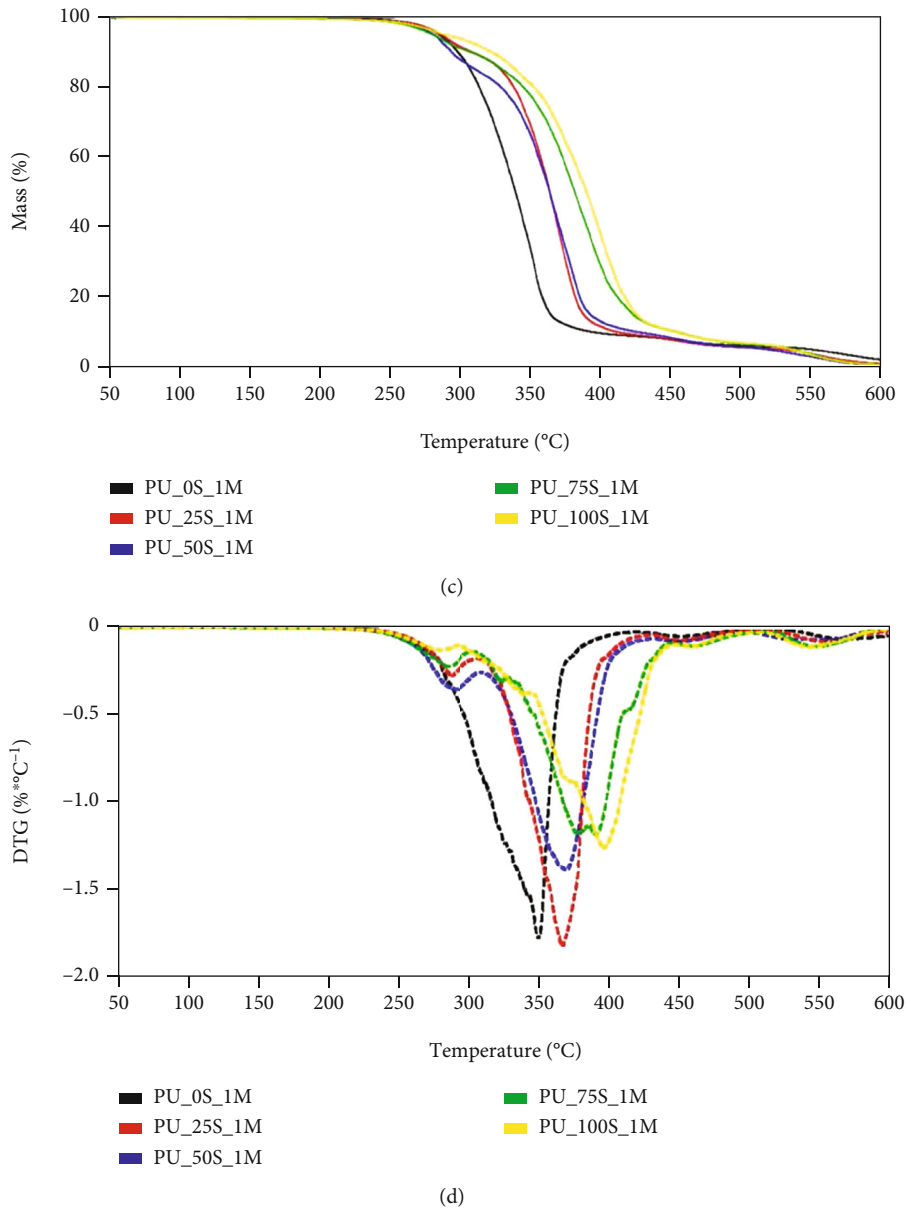

Figure 6: TG and DTG curves of PU/starch composites without (a, b) magnetite and (c, d) with 1% magnetite.

characteristic bands such as strong absorption of N–H stretching vibrations (3343 cm^{-1}), symmetrical and asymmetrical C-H stretching vibrations of CH_2 groups (2864 cm^{-1} and 2944 cm^{-1}, respectively), the main absorption band of the C=O carbonyl group (1723 cm^{-1}), C–N stretching vibrations (1415 cm^{-1}), C–H bending vibrations of the CH_3 groups (1365 cm^{-1}) [22]. Furthermore, for polyurethane spectra with magnetite addition, a characteristic band of approximately 590 cm^{-1} was also observed, corresponding to the vibrations of the Fe-O functional group [23].

The addition of starch did not cause significant changes in the position of individual absorption bands, but it influenced the intensity of some of them. With an increasing amount of added starch, the main absorption band of the C=O carbonyl group decreases. The addition of starch also reduces the intensity of the bands corresponding to the N-H stretching vibrations and the symmetric and asymmetric C-H stretching vibrations of the CH_2 groups.

The addition of magnetite also did not lead to major changes in the absorption bands. Only the bands corresponding to the asymmetric C-O stretching vibrations slightly shifted towards lower values of the wavenumbers with the increase of the content of the magnetic particles. Additionally, a new band appeared corresponding to the vibrations of the Fe-O functional group (approx. 590 cm^{-1}); however, no relationship was found between the addition of magnetite and the intensity of individual bands.

FTIR spectra in the range 1650-1800 cm^{-1} were deconvolved using OPUS software to obtain the peak area of the C=O groups bound by hydrogen bonds at 1694-1712 cm^{-1}

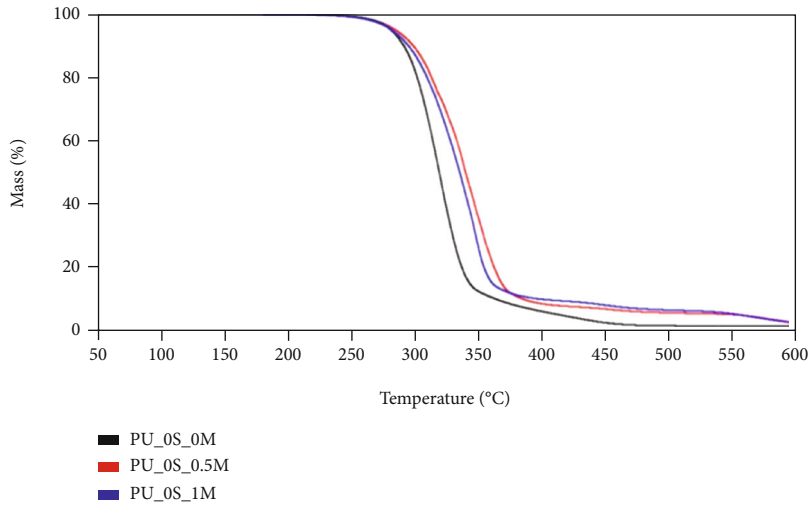

(a)

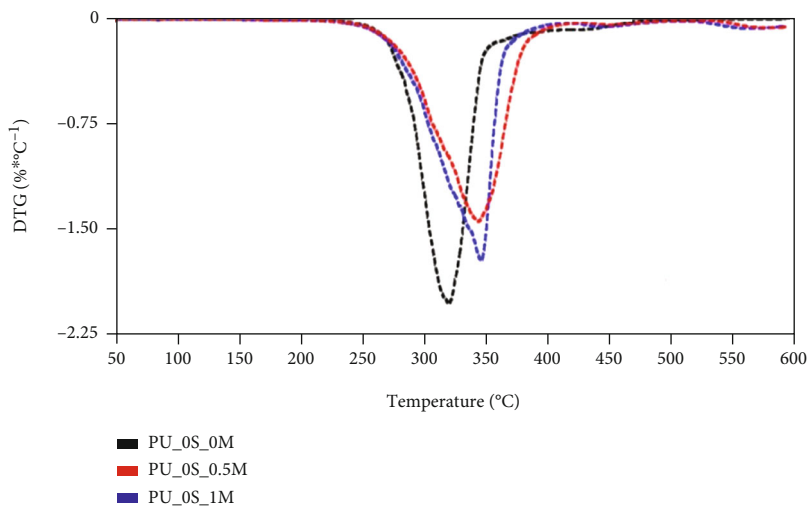

(b)

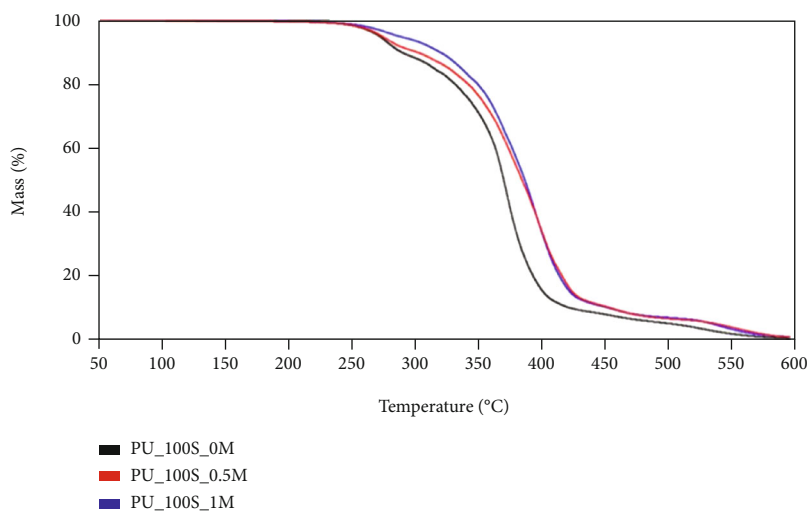

(c)

Figure 7: Continued.

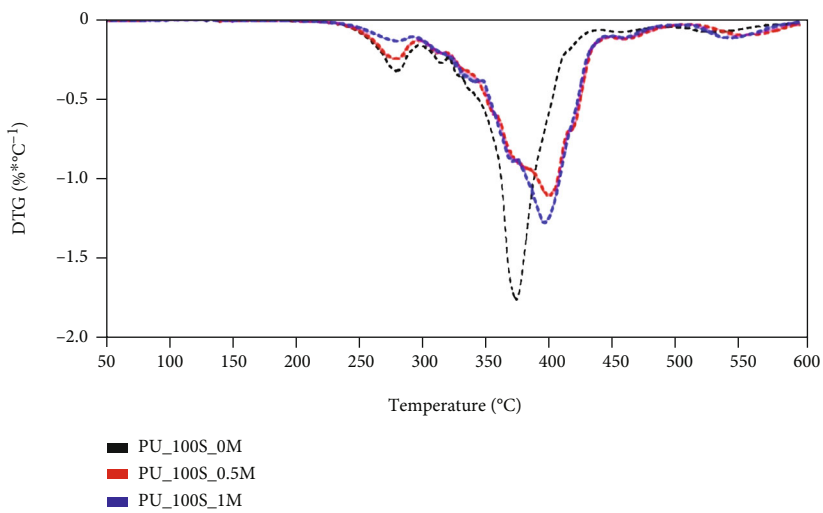

(d)

Figure 7: TG and DTG curves of PU/magnetite composites without (a, c) starch and (b, d) with 100% starch.

Table 4: TG results of PU/starch/magnetite composites.

Sample code	$T_{1\%}$ (°C)	$T_{2\%}$ (°C)	$T_{3\%}$ (°C)	$T_{10\%}$ (°C)	$T_{50\%}$ (°C)	T_{DTGmax} (°C)	M_{resid} (%)
Magnetite	—	—	—	—	—	312	99.295
Starch	274	281	285	296	312	307	13.041
PU_0S_0M	253	267	274	291	319	322	1.284
PU_25S_0M	246	261	268	289	353	368	0
PU_50S_0M	253	268	277	307	366	363	3.266
PU_75S_0M	240	257	266	291	347	355	0.512
PU_100S_0M	238	254	261	289	369	372	0.489
PU_0S_1M	251	264	272	294	335	347	2.489
PU_25S_1M	251	265	273	305	359	363	1.384
PU_50S_1M	246	260	268	290	359	374	1.174
PU_75S_1M	240	256	265	304	377	379	1.172
PU_100S_1M	244	261	271	319	386	393	1.128
PU_0S_0.5M	255	267	275	298	340	339	2.585
PU_100S_0.5M	238	255	263	301	384	396	0.993

in urethane structures and from the free C=O group at 1711-1730 cm^{-1} Figure 4. Based on the results of deconvolution, the degree of hydrogen bonding and the degree of phase separation in the obtained polyurethanes were calculated. The degree of carbonyl groups that participate in hydrogen bonding can be described by the carbonyl hydrogen bond ratio R, which can be determined from the equation [24–26]

$$R = \frac{C_{bonded} * f_{bonded}}{C_{free} * f_{free}} = \frac{A_{1694-1712}}{A_{1711-1730}}, \quad (1)$$

where C is the concentration, A is the area of the absorption peak, and f is the respective extinction coefficient of the bonded and free carbonyl groups.

The phase separation degree (DPS) was calculated using the following equation:

$$\mathrm{DPS} = \frac{C_{bonded}}{C_{free} + C_{bonded}} = \frac{R}{1 + R}. \quad (2)$$

Figure 4 presents an exemplary result of the deconvolution of the IR C=O absorption band, and phase separation data are collected in Table 3.

Based on the results of phase separation summarized in Table 3, it can be concluded that polyurethanes without the addition of starch exhibit the highest phase separation. They are characterized by the highest values of the carbonyl hydrogen bonding index and therefore also by the degree of phase separation. The high degree of phase separation of PUs results from their segmented structure. The PU chains

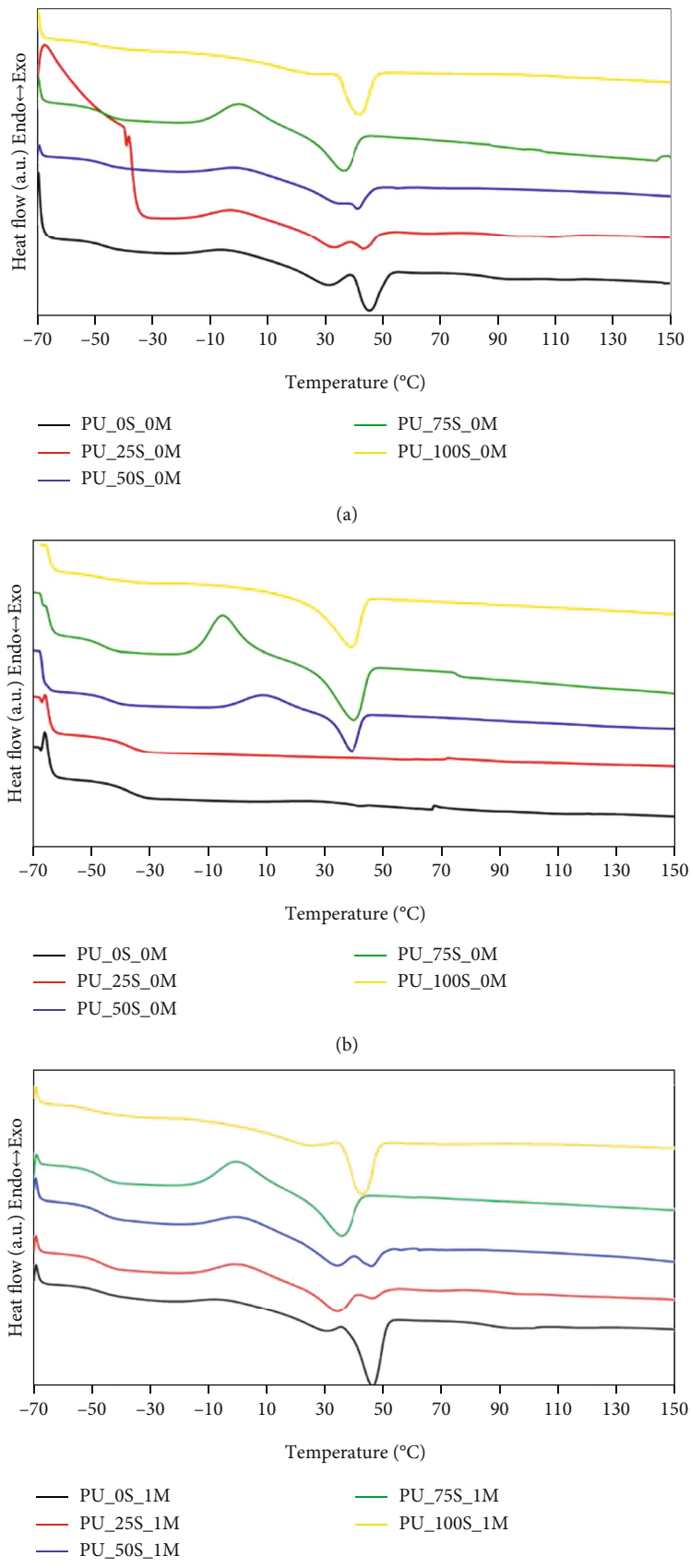

Figure 8: Continued.

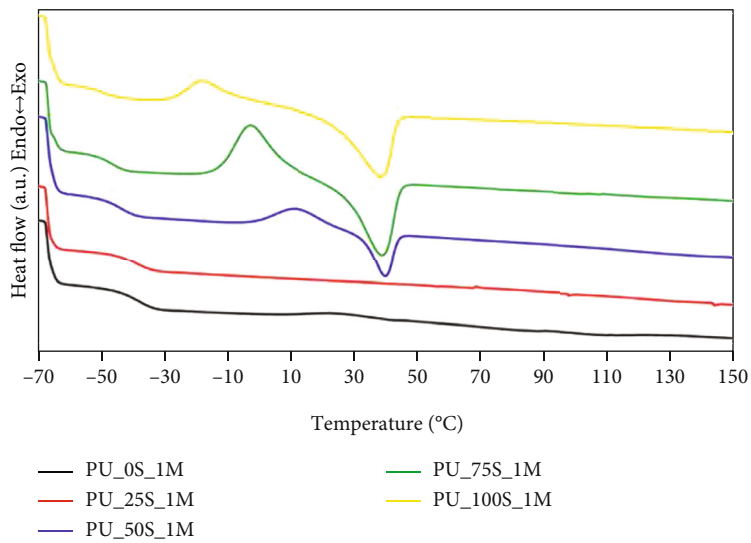

(d)

Figure 8: DSC profiles of PU composites with different amounts of starch with (a, b) magnetite and without (c, s) magnetite; (a, c) first and (b, d) second heating run.

are made of alternating soft and hard segments. The soft segments are most often composed of polyesters, which show polar characteristics. On the other hand, the hard segments consist most often of nonpolar hydrocarbon structures derived from diisocyanates and polar isocyanate groups. The combination of segments with different polarities causes difficulties in mixing them. As a result, PU with a high degree of phase separation is formed. However, in composite materials, the incorporated modifiers can hinder segmental mobility and, consequently, cause a reduction in the degree of phase separation [7].

Among the samples with the addition of starch, it can also be seen that the degree of phase separation increases with the increase in the amount of starch added. This means that polyurethanes that contain only starch or PDO show the highest phase separation. In the case of systems containing both starch and PDO, the degree of phase separation is lower. This can be connected to the limited chain mobility in the more complex system. It is hard to draw clear conclusions about the influence of magnetic particles on the degree of phase separation. In the group without starch, with the addition of magnetite DPS decreases; in the samples with 100% starch, these values are diverse. The thermogravimetric curves are presented in Figures 5–7; data are collected in Table 4.

The TG and DTG results show that magnetite is stable over the entire temperature range. Starch is less stable because it starts to degrade at quite low temperatures. The temperature of the maximum mass loss was only 307°C.

The results obtained suggest that the addition of starch to the system decreases the characteristic temperatures of the polyurethanes obtained and the material exhibits lower thermal stability. This change does not depend on the presence of magnetic particles, as a similar correlation was observed in both groups. The curves obtained also show that in the case of samples with the addition of starch, before the main stage of thermal degradation, there is one more small peak, most likely the result of the degradation of this polysaccharide. On the other hand, at about 500°C, there are maxima related to the decomposition of the residues [27]. Moreover, it can be seen that for materials containing a higher amount of starch, the temperature of maximum weight loss is higher.

However, the addition of magnetic particles does not have a significant effect on the thermal stability of the obtained polyurethanes. Regardless of the composition of the basic system, the characteristic temperatures did not change significantly with an increasing amount of magnetite. However, a slight increase in the temperature of the maximum weight loss was found in the samples containing magnetic particles.

Figures 8 and 9 present DSC curves of PU compounds, and data are collected in Table 5.

The addition of starch caused a decrease in the glass transition temperature, which may indicate that starch acts as a plasticizer for soft segments [28]. At temperatures around 0°C, in some cases, peaks can also be seen as a result of the cold crystallization process. The glass transition of hard segments is difficult to determine because it superimposes the melting of soft segments, which results in "double melting peaks" in some samples. Only in the case of samples containing 100% starch was it possible to determine the parameters of the glass transition process of hard segments. The melting temperature of the soft segments decreases with increasing starch addition, except for samples containing 100% polysaccharide. Because of the crosslinking of starch and thus the need to provide more energy, the enthalpy of fusion should increase with increasing amount. However, it is not directly visible in the results, most probably due to the glass transition of the hard segments that overlap this

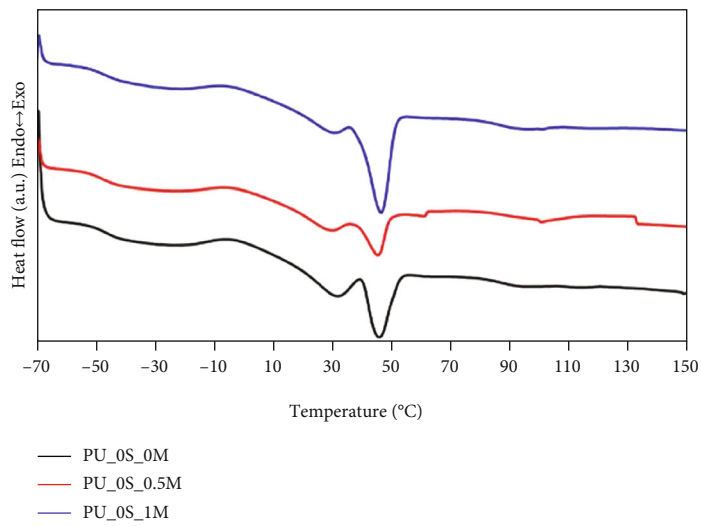

(a)

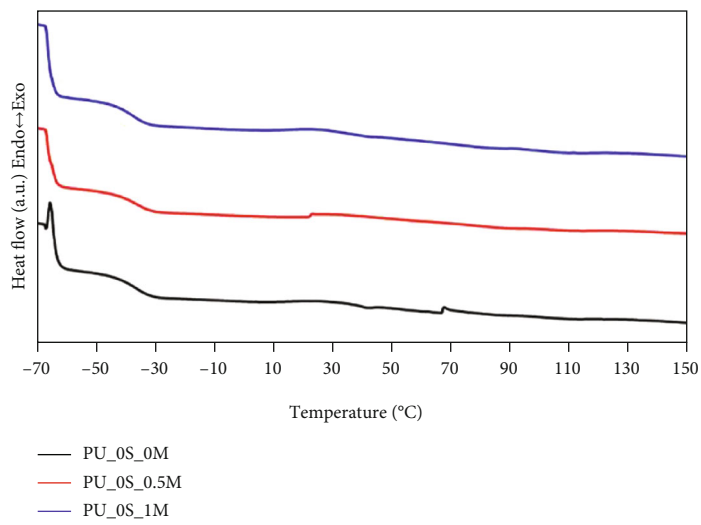

(b)

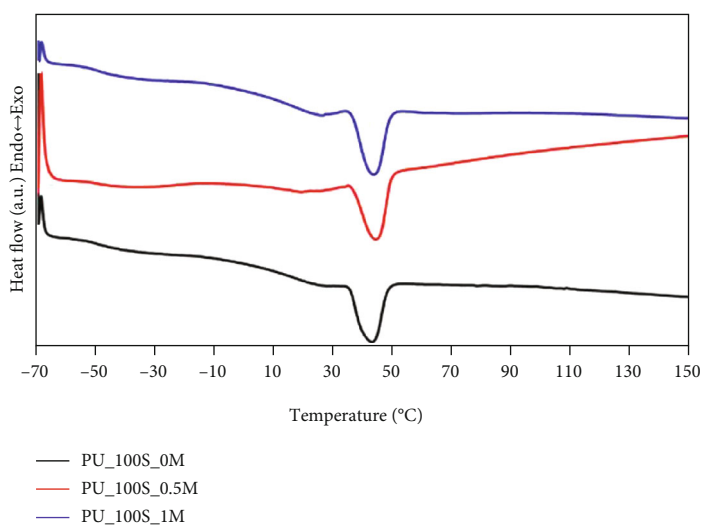

(c)

Figure 9: Continued.

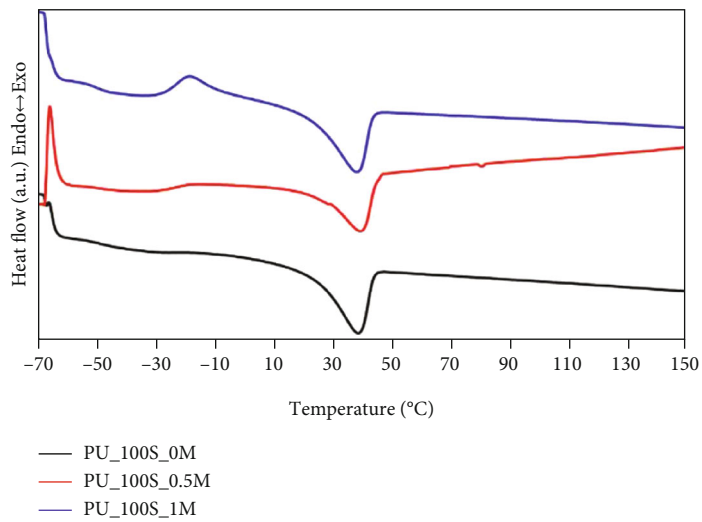

(d)

Figure 9: DSC profiles of PU composites with different amounts of magnetite with (a, b) starch and (c, d) without starch; (a, c) first and (b, d) second heating run.

phase change. During the second heating run, the glass transition temperatures are higher, while the effect of starch does not change. Moreover, for the first two samples, no distinct peaks correspond to the melting of soft segments, which is most likely the result of the limited crystallization of this phase. The melting parameters of hard segments can only be determined for materials containing small amounts of starch. The presence of two glass transitions and two melting processes in individual samples confirms the presence of two types of segments (soft and hard) with limited miscibility.

It was found that the addition of magnetite causes a minimal increase in the glass transition temperature of the soft segments. During the first heating run of the samples at temperatures slightly below 0°C, exothermic peaks characteristic of cold crystallization appear. The addition of magnetic particles does not significantly affect the melting temperature of soft segments. During the second heating run, the glass transition temperatures of the soft segments are slightly higher than during the first one. The heat capacity for most samples is lower during the second heating run.

The thermal analysis of DMA enables determination of the damping coefficient—tangent of the loss angle (δ)—and is expressed by the relationship

$$\tan \delta = \frac{E''}{E'}, \tag{3}$$

where E'' is the loss modulus and E' is the storage modulus.

The maximum in the curve that expresses the dependence of tan δ as a function of temperature corresponds to the glass transition temperature of the polymer, but it differs from that determined by the DSC method [29, 30].

The DMA results are presented in Figure 10, and the data are collected in Table 6.

It is difficult to notice the dependence between the amount of starch added and the glass transition temperatures of the hard and soft segments in the obtained polyurethanes. The glass transition of soft segments takes place at a temperature of approximately -15° C, while for hard segments it is approximately 35°C. Below the glass transition temperature, the tangent δ is very small, which is the result of the state of being of the material. In the glassy state, the mobility of the polymer chains is "frozen," which means that the material accumulates more energy and dissipates at a low level. With increasing temperature and thus changing the state of the material, the value of the tangent δ also increases. This is the result of the higher mobility of polymer chains in the elastic state.

It is also not straightforward to determine the relationship between the amount of magnetite added and the glass transition temperatures of individual segments in the obtained polyurethanes. Between the temperatures corresponding to the glass transition of individual segments, the so-called plateau, this is the range in which the material exhibits elastic properties. As in the case of the first two groups below the glass transition temperature, the tangent value of the loss angle is very small, which results from the glassy state in which the material is located. After the glass transition, as the material becomes more elastic, the damping factor gradually increases.

Above the glass transition temperature of the hard segments, the storage modulus for most samples is slightly lower than at the beginning of the study, which is a result of the greater freedom of movement of the polymer chains. Figures 11 and 12 present the results of the ultrasonic tests.

In the group of samples modified with starch, the increase in the polysaccharide content causes an increase

Table 5: DSC results of PU/starch/magnetite composites.

	Sample code	Glass transition of soft segments		Melting of soft segments		Cold crystallization		Glass transition of hard segments		Melting of hard segments	
		T_{g1} (°C)	ΔCp (J∗g^{-1})	T_{m1} (°C)	ΔH (J∗g^{-1})	T_c (°C)	ΔC (W∗g^{-1})	T_{g2} (°C)	ΔCp (J∗g^{-1})	T_{m2} (°C)	ΔH (J∗g^{-1})
1 heating run	PU_0S_0M	-44	0.606	45	16.4	-6	0.15	—	—	93	2.2
	PU_25S_0M	-47	2.263	43	10.9	-3	0.19	—	—	97	2
	PU_50S_0M	-46	0.507	41	12.9	-1	0.27	—	—	—	—
	PU_75S_0M	-46	0.591	36	11.7	0	0.17	—	—	108	1.7
	PU_100S_0M	-49	0.255	42	13	—	—	20	0.199	—	—
	PU_0S_1M	-39	0.366	46	20.6	-8	0.27	—	—	96	3.2
	PU_25S_1M	-45	0.524	34	8.5	-1	0.26	—	—	93	1.1
	PU_50S_1M	-47	0.317	34	7.9	-1	0.29	—	—	—	—
	PU_75S_1M	-47	0.387	35	14.1	-1	0.19	—	—	—	—
	PU_100S_1M	-48	0.238	43	14.1	—	—	19	0.351	—	—
	PU_0S_0.5M	-45	0.332	45	11.8	-8	0.27	—	—	—	—
	PU_100S_0.5M	-48	0.039	44	12.3	—	—	27	0.298	—	—
2 heating run	PU_0S_0M	-36	0.409	—	—	—	—	—	—	—	—
	PU_25S_0M	-37	0.372	—	—	—	—	—	—	—	—
	PU_50S_0M	-44	0.418	39	11.8	8	0.22	—	—	—	—
	PU_75S_0M	-45	0.333	39	21	-5	0.05	—	—	—	—
	PU_100S_0M	-35	0.331	39	22.3	—	—	—	—	—	—
	PU_0S_1M	-36	0.275	—	—	—	—	—	—	109	0.8
	PU_25S_1M	-38	0.029	—	—	—	—	—	—	—	—
	PU_50S_1M	-42	0.321	40	7.2	11	0.28	—	—	—	—
	PU_75S_1M	-44	0.224	39	19.2	-3	0.09	—	—	—	—
	PU_100S_1M	-44	0.109	38	24.4	-18	0.21	—	—	—	—
	PU_0S_0.5M	-37	0.419	—	—	—	—	—	—	89	1.1
	PU_100S_0.5M	-46	0.347	40	17.4	—	—	—	—	—	—

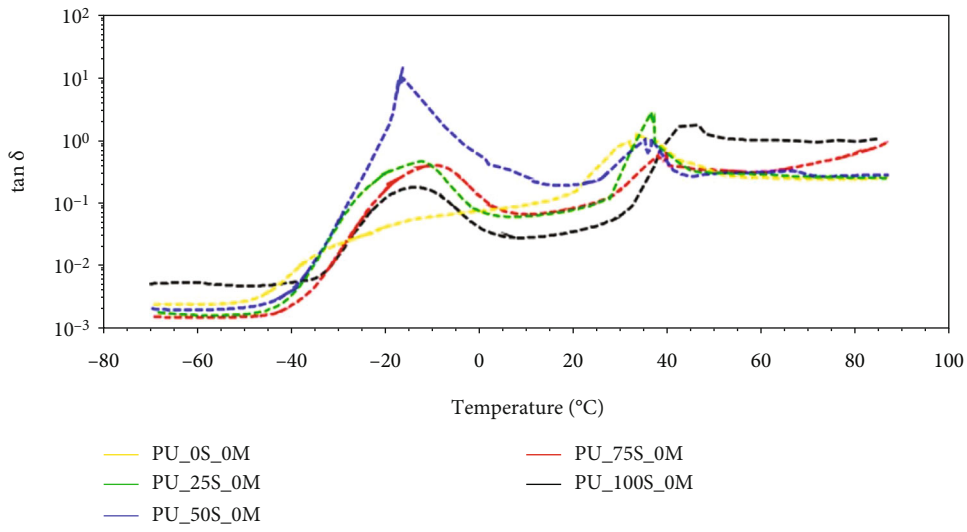

(a)

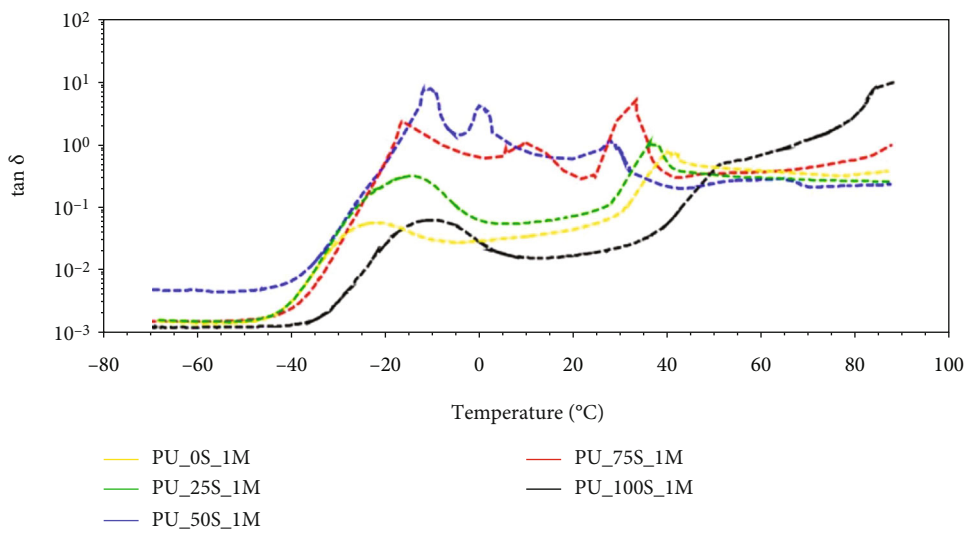

(b)

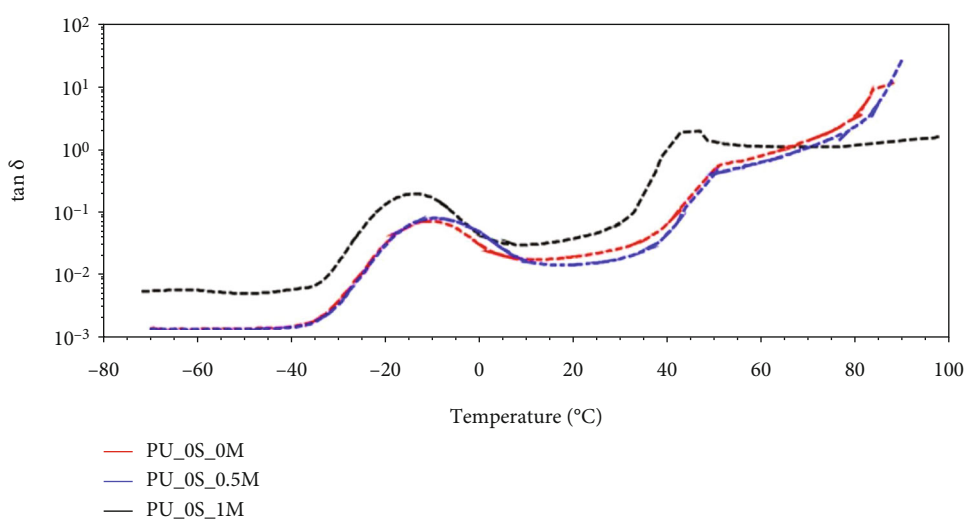

(c)

Figure 10: Continued.

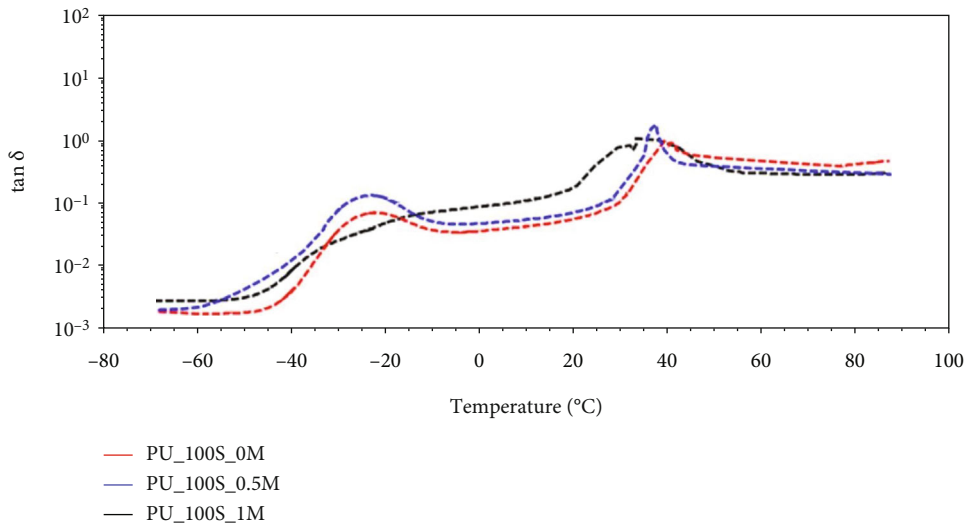

(d)

Figure 10: DMA curves of PU composites with different amounts of (a, b) starch or (c, d) magnetite.

Table 6: DMA results: glass transition temperatures of soft (T_{g1}) and hard (T_{g2}) segments for PU/starch/magnetite composites.

Sample code	T_{g1} (°C)	T_{g2} (°C)
PU_0S_0M	-14	43
PU_25S_0M	-10	38
PU_50S_0M	-17	36
PU_75S_0M	-13	36
PU_100S_0M	—	32
PU_0S_1M	-10	—
PU_25S_1M	-17	33
PU_50S_1M	-11	30
PU_50S_1M	-15	36
PU_100S_1M	-22	39
PU_0S_0.5M	-9	—
PU_100S_0.5M	-23	37

(about 10%) of the longitudinal ultrasonic wave velocity from $V_L = 369.2$ m/s (PU_0S_0M) to $V_L = 406.3$ m/s (PU_100S_0M) in Figure 11(a). The increase in velocity for PU with a 25% addition of starch is due to the greater plasticity of the sample, so when measuring the velocity, it was necessary to use greater pressure of the heads (to allow the passage of the ultrasonic wave), and as a result, slightly higher velocity results were obtained.

Additionally, in the case of a group of samples with 1% magnetite admixture, along with an increase in their polysaccharide content, there is an increase (approx. 11%) of the longitudinal ultrasonic wave velocity from $V_L = 377.3$ m/s (PU_0S_1M) to 422.6 m/s (PU_100S_1M) in Figure 11(b). The higher values of the wave velocity obtained for PU_50S_1M are related to the greater plasticity of the sample.

For the group of samples modified with magnetite from 0% to 1% (without starch), the velocity of longitudinal ultrasonic wave propagation slightly increases (up to 3%) from $V_L = 369.2$ m/s (PU_0S_0M) to $V_L = 377.3$ m/s (PU_0S_1M) in Figure 11(c).

Similarly, for samples with 100% starch addition in Figure 11(d), the modification with magnetite causes an increase of 4% of the propagation speed of the longitudinal ultrasonic wave from $V_L = 406.3$ m/s (PU_100S_0M) to $V_L = 422.6$ m/s (PU_100S_1M).

In both groups of magnetite modified samples, for samples containing 0.5% magnetite (without starch and with 100% starch addition) Figures 11(c) and 11(d), the highest velocity values were obtained, respectively, $V_L = 388.1$ m/s (PU_0S_0.5 M) and $V_L = 451.2$ m/s (PU_100S_0.5M). It is related to the greater plasticity of these samples. The apparent density study also showed an increase in apparent density depending on the addition of magnetite for both groups of samples (Figures 12(a) and 12(b)), which is consistent with the rectilinear relationship between the velocity of the longitudinal ultrasonic wave and the apparent density.

Ultrasonic tests conducted on modified PUs with starch and magnetite showed that the increase in the speed of propagation of longitudinal ultrasonic waves up to 11% is mainly related to the amount of polysaccharide added. The effect of the addition of magnetite (without starch) is smaller and does not exceed 5%.

The observed increase in wave velocity is responsible for a correspondingly higher Young's modulus, i.e., elasticity of a given material. The tested samples, along with the growth of modifiers, are characterized by greater elasticity and therefore material stiffness.

In Figure 13, microscopic images show the surface morphology of polyurethane materials. The polyurethane shown in Figure 13(d) has a relatively smooth surface, indicating a tight architecture of the crosslinked PU. On the other hand,

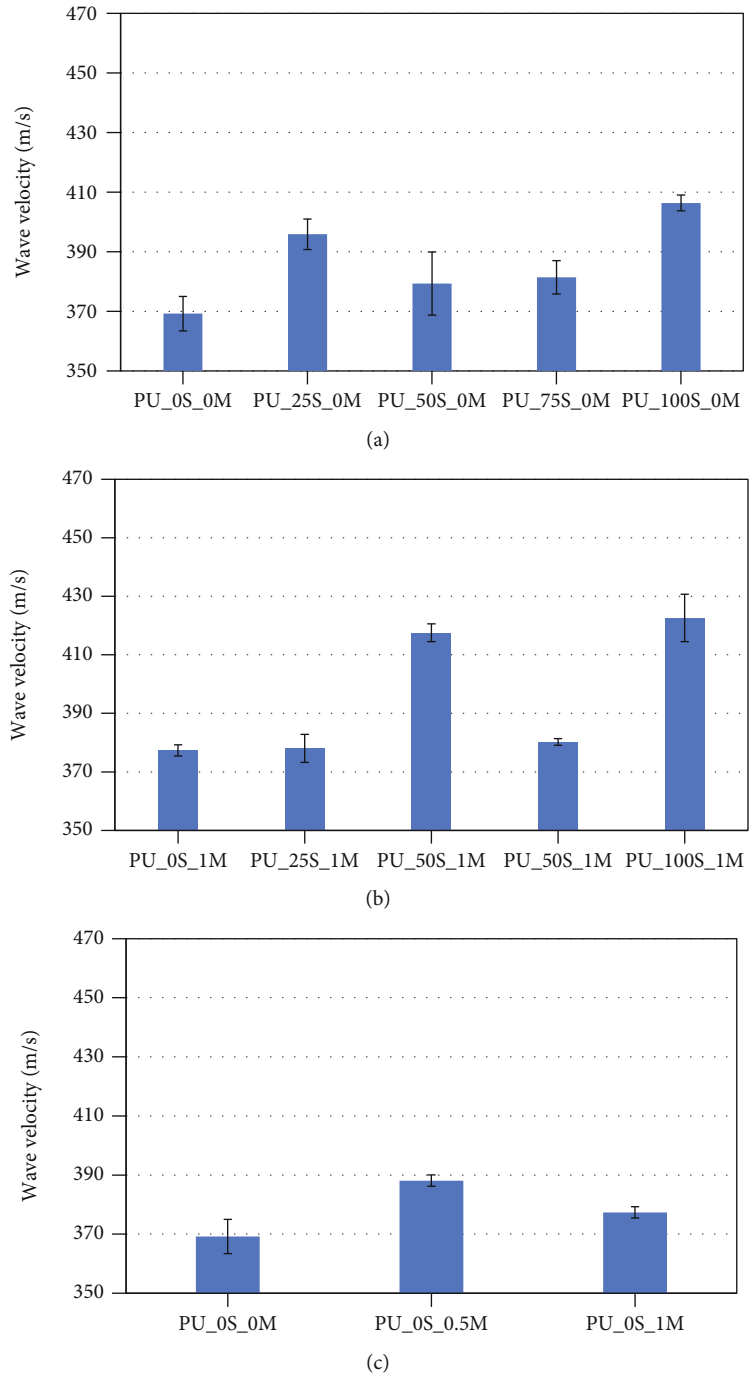

Figure 11: Continued.

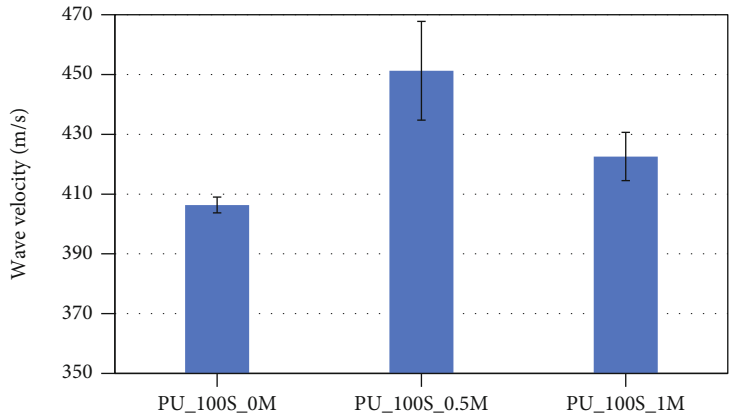

(d)

Figure 11: Ultrasonic wave velocity for PU with different starch content (a) without magnetite and (b) with 1% of magnetite and for PU with different magnetite content (c) without the addition of starch and (d) with 100% of starch.

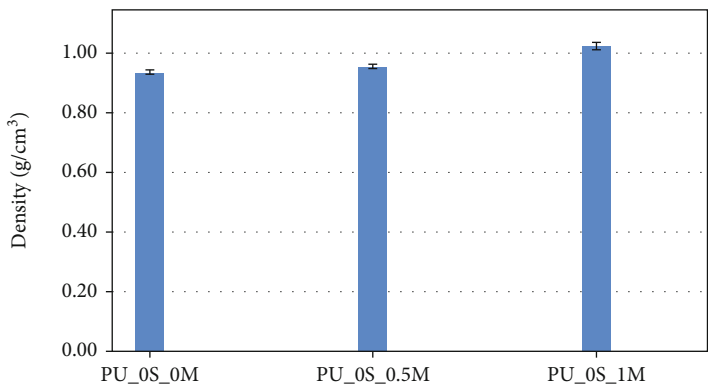

(a)

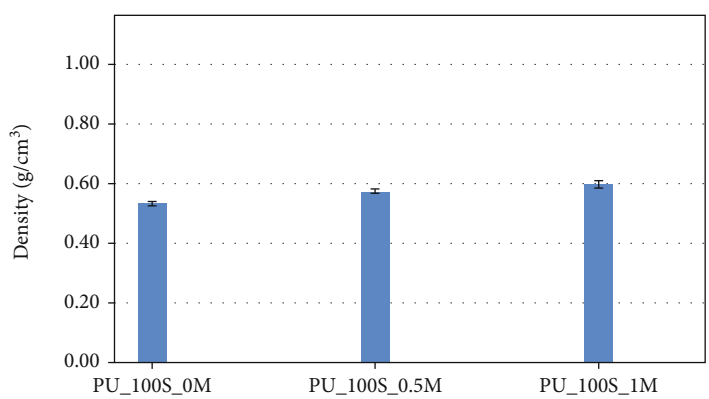

(b)

Figure 12: The apparent density of PU with different magnetite content (a) without the addition of starch and (b) with 100% starch.

samples that contain the addition of starch are slightly cracked, which is the result of a less dense polyurethane network. Blurry white points indicate the location of magnetic particles inside the polymer matrix. Their presence is confirmed by the average EDS analysis of the surface of the material. In the case of point analysis at higher magnification (Figure 13(c)), individual magnetite grains can be specifically identified. EDS analysis of the obtained materials showed the presence of iron, but otherwise, the material consists mainly of carbon and oxygen.

Figure 14 shows the result of SEM analysis of the surface of the tested samples, which show changes in morphology after incubation in SBF. On the surface of polyurethanes, numerous structures of formed apatite, as well as sodium

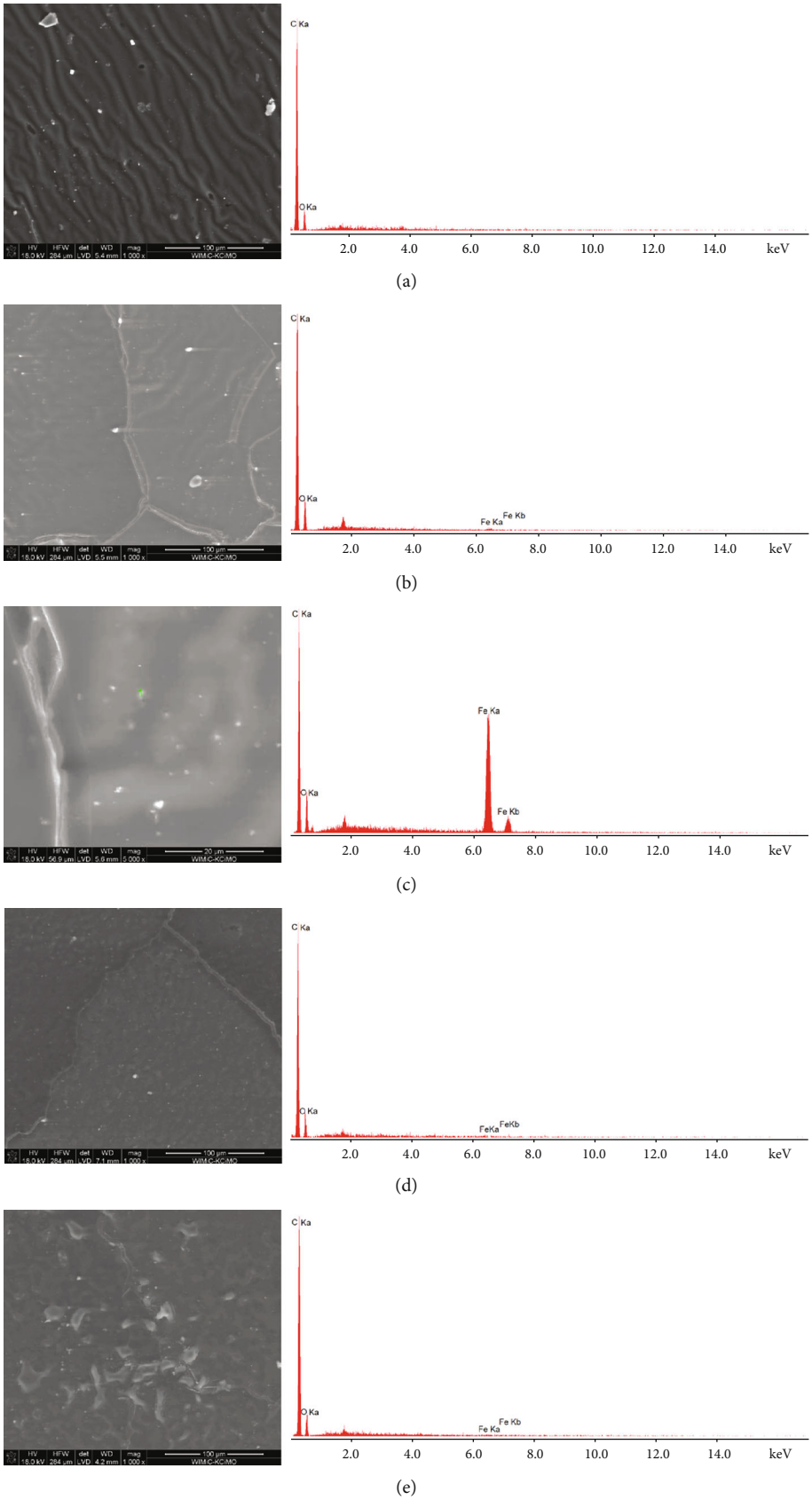

Figure 13: SEM microphotographs of PU modified with starch and magnetite and the results of EDS average analysis: (a) PU_25S_0M, (b) PU_25S_1M, (c) PU_25S_1M, (d) PU_0S_1M, and (e) PU_100S_0.5M.

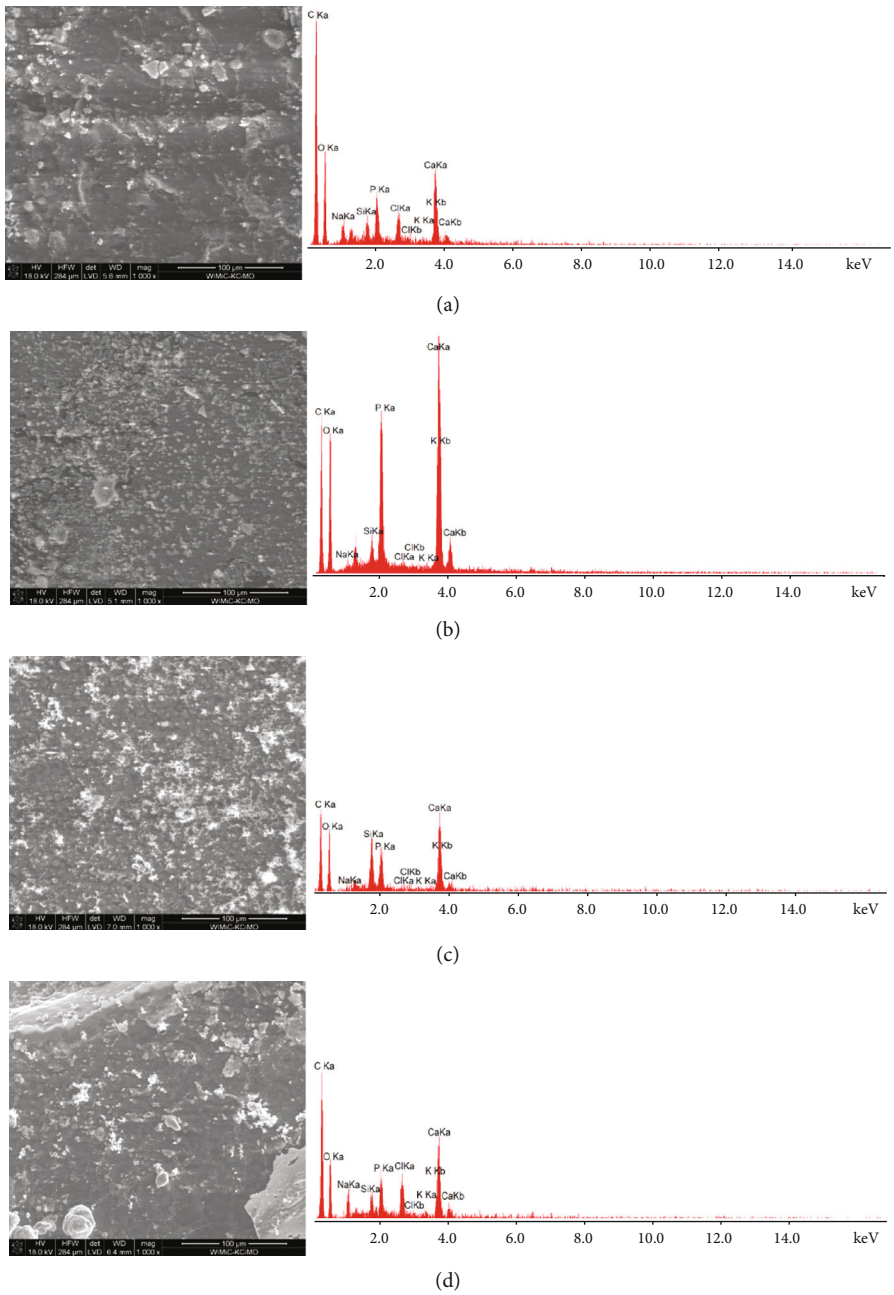

Figure 14: SEM microphotographs of PU modified with starch and magnetite and the results of the EDS average analysis after 25 days of incubation in SBF: (a) PU_100S_0M, (b) PU_50S_1M, (c) PU_0S_1M, and (d) PU_100S_1M.

chloride and carbonates, are visible. EDS spectra confirm the presence of apatites (hydroxyapatite layer) as increased amounts of calcium and phosphorus can be seen.

4. Conclusions

The subject of the work was modified polyurethanes obtained by a one-step method. Samples with different contents of additives, starch, and magnetite were synthesized and characterized in terms of structure and morphology. FTIR spectroscopy confirmed the structure of the polyurethanes obtained. The introduction of starch into the system did not change the position of individual absorption bands, but it did affect the intensity of some of them. With an increasing amount of polysaccharide, the intensity of the main absorption band of the carbonyl group C=O, the band corresponding to the N-H stretching vibrations, and the symmetric and asymmetric CH stretching bands of the CH_2 groups decreased. The degree of phase separation is the highest for PU without starch, but with increasing amounts of modifier, it also increases. The bioactivity study confirmed that the obtained polyurethanes show the ability to create apatite on their surface. It has been found that PUs containing starch showed lower thermal stability. The

addition of starch decreased the glass transition temperature of the soft segments, which may indicate that it acts as a plasticizer. DSC analysis showed that the addition of starch causes a decrease in the melting point of the soft segments of polyurethanes and an increase in the heat of fusion, most likely due to crosslinking by the polysaccharide.

The addition of magnetic particles did not cause such large changes in the properties of the obtained PU materials as starch. The thermal stability determined by TG did not practically change; as with the addition of starch, magnetite also accelerated the glass transition process. However, the magnetic particles did not affect the melting point of the soft segments. The addition of magnetite did not significantly affect the position of the absorption bands in the FTIR analysis. Only a new absorption band was noticed, corresponding to the vibrations of the Fe-O functional group (approx. 590 cm^{-1}). The images obtained by SEM showed single magnetite grains, which were also identified using EDS analysis. The study of bioactivity showed a similar result as in the case of samples with the addition of starch, which proves that the magnetic particles do not affect the bioactivity of the obtained polyurethanes. After incubation in SBF, a hydroxyapatite layer was formed on the surface of the modified polyurethanes.

In conclusion, the obtained materials are characterized by good thermal properties—a key feature for hyperthermia applications—as well as show potential bioactivity, which will probably lead to osseointegration with bone tissue and make them useful fillings for bone defects in orthopedics.

Data Availability

All the data used to support the findings of this study are included within the article.

Conflicts of Interest

The authors declare that they have no conflicts of interest.

Acknowledgments

The authors are grateful to the Polish National Science Centre for financial support under the Contract No. UMO-2016/22/E/ST8/00048. This work was supported by a subsidy from the Ministry of Education and Science for the AGH University of Science and Technology in Kraków (Project No. 16.16.160.557). MSz has been partially supported by the EU Project POWR.03.02.00-00-I004/16.

References

[1] M. Meskinfam, S. Bertoldi, N. Albanese et al., "Polyurethane foam/nano hydroxyapatite composite as a suitable scaffold for bone tissue regeneration," *Materials Science and Engineering: C.*, vol. 82, no. 82, pp. 130–140, 2018.

[2] M. Sultan, "Hydroxyapatite/polyurethane composites as promising biomaterials," *Chemical Papers.*, vol. 72, no. 10, pp. 2375–2395, 2018.

[3] P. Szczepańczyk, K. Pazdan, K. Pielichowska, and J. Chłopek, *Biomedical implants for bone tissue replacement and regeneration*, Properties and Applications, Green Polymer Composites Technology, 2016.

[4] K. Pielichowska and S. Blazewicz, "Bioactive polymer/hydroxyapatite (nano)composites for bone tissue regeneration," *Advances in Polymer Science.*, vol. 232, 2010.

[5] J. P. Santerre, K. Woodhouse, G. Laroche, and R. S. Labow, "Understanding the biodegradation of polyurethanes: from classical implants to tissue engineering materials," *Biomaterials*, vol. 26, no. 35, pp. 7457–7470, 2005.

[6] S. Kim and S. Liu, "Smart and biostable polyurethanes for long-term implants," *ACS Biomaterials Science & Engineering.*, vol. 4, no. 5, pp. 1479–1490, 2018.

[7] P. Król, "Synthesis methods, chemical structures and phase structures of linear polyurethanes. Properties and applications of linear polyurethanes in polyurethane elastomers, copolymers and ionomers," *Progress in Materials Science*, vol. 52, no. 6, pp. 915–1015, 2007.

[8] P. Szczepańczyk, K. Pielichowska, and J. Chłopek, "Polyurethane composite foams with β-tricalcium phosphate for biomedical applications," *Journal of Reinforced Plastics and Composites.*, vol. 34, no. 22, pp. 1856–1870, 2015.

[9] F. Zia, K. M. Zia, M. Zuber, S. Kamal, and N. Aslam, "Starch based polyurethanes: a critical review updating recent literature," *Carbohydrate Polymers.*, vol. 134, pp. 784–798, 2015.

[10] A. L. Da Róz, A. A. S. Curvelo, and A. Gandini, "Preparation and characterization of cross-linked starch polyurethanes," *Carbohydrate Polymers.*, vol. 77, no. 3, pp. 526–529, 2009.

[11] M. Bil, J. Ryszkowska, P. Woźniak, K. J. Kurzydłowski, and M. Lewandowska-Szumieł, "Optimization of the structure of polyurethanes for bone tissue engineering applications," *Acta Biomaterialia*, vol. 6, no. 7, pp. 2501–2510, 2010.

[12] Y. Ma, N. Hu, J. Liu et al., "Three-dimensional printing of biodegradable piperazine-based polyurethane-urea scaffolds with enhanced osteogenesis for bone regeneration," *ACS Applied Materials & Interfaces.*, vol. 11, no. 9, pp. 9415–9424, 2019.

[13] M. Barikani, H. Honarkar, and M. Barikani, "Synthesis and characterization of polyurethane elastomers based on chitosan and poly(ε-caprolactone)," *Journal of Applied Polymer Science.*, vol. 112, no. 5, pp. 3157–3165, 2009.

[14] A. Ito, M. Shinkai, H. Honda, and T. Kobayashi, "Medical application of functionalized magnetic nanoparticles," *Journal of Bioscience and Bioengineering*, vol. 100, no. 1, pp. 1–11, 2005.

[15] M. I. Anik, M. K. Hossain, I. Hossain, A. M. U. B. Mahfuz, M. T. Rahman, and I. Ahmed, "Recent progress of magnetic nanoparticles in biomedical applications: a review," *Nano Select.*, vol. 2, no. 6, pp. 1146–1186, 2021.

[16] M. Pawlaczyk and G. Schroeder, "Hybrydowe nanomateriały magnetyczne," *Cursiva*, 2017.

[17] M. Shinkai, "Functional magnetic particles for medical application," *Journal of Bioscience and Bioengineering*, vol. 94, no. 6, pp. 606–613, 2002.

[18] R. V. Ramanujan, "Magnetic particles for biomedical applications," in *Biomedical Materials*, pp. 477–491, In: Springer US, 2009.

[19] M. Chalid, M. J. H. Masrudin, and J. H. Mustafa, "Study of nano-Fe₃O₄ addition on magnetic and mechanical properties of HMDI-based polyurethane," *Materials Science Forum*, vol. 894, pp. 25–28, 2017.

[20] H. Zou, C. Weder, and Y. C. Simon, "Shape-memory polyurethane nanocomposites with single layer or bilayer oleic acid-

coated Fe3O4 nanoparticles," *Macromolecular Materials and Engineering*, vol. 300, no. 9, pp. 885–892, 2015.

[21] T. Kokubo and H. Takadama, "How useful is SBF in predicting in vivo bone bioactivity?," *Biomaterials*, vol. 27, no. 15, pp. 2907–2915, 2006.

[22] A. Mohammadi, M. Barikani, and M. Barmar, "Synthesis and investigation of thermal and mechanical properties of in situ prepared biocompatible Fe3O4/polyurethane elastomer nanocomposites," *Polymer Bulletin.*, vol. 72, no. 2, pp. 219–234, 2015.

[23] L. Yang, J. Tian, J. Meng et al., "Modification and characterization of Fe3O4 nanoparticles for use in adsorption of alkaloids," *Molecules*, vol. 23, no. 3, p. 562, 2018.

[24] P. Król, Ł. Uram, B. Król, K. Pielichowska, M. Sochacka-Piętal, and M. Walczak, "Synthesis and property of polyurethane elastomer for biomedical applications based on nonaromatic isocyanates, polyesters, and ethylene glycol," *Colloid and Polymer Science.*, vol. 298, no. 8, pp. 1077–1093, 2020.

[25] R. W. Seymour, G. M. Estes, and S. L. Cooper, "Infrared studies of segmented polyurethan elastomers. I. Hydrogen bonding," *Macromolecules*, vol. 3, no. 5, pp. 579–583, 1970.

[26] G. M. Estes, R. W. Seymour, and S. L. Cooper, "Infrared studies of segmented polyurethane elastomers. II. Infrared dichroism," *Macromolecules*, vol. 4, no. 4, pp. 452–457, 1971.

[27] M. Szlachta, K. Ordon, K. Nowicka, and K. Pielichowska, "Thermal properties of polyurethane-based composites modified with chitosan for biomedical applications," *Journal of Thermal Analysis and Calorimetry.*, vol. 143, no. 5, pp. 3471–3478, 2021.

[28] A. S. A. Hazmi, N. N. P. N. Pauzi, Z. A. Maurad et al., "Understanding intrinsic plasticizer in vegetable oil-based polyurethane elastomer as enhanced biomaterial," *Journal of Thermal Analysis and Calorimetry.*, vol. 130, no. 2, pp. 919–933, 2017.

[29] C. A. Gracia-Fernández, S. Gómez-Barreiro, J. López-Beceiro, J. Tarrío Saavedra, S. Naya, and R. Artiaga, "Comparative study of the dynamic glass transition temperature by DMA and TMDSC," *Polymer Testing.*, vol. 29, no. 8, pp. 1002–1006, 2010.

[30] W. Sun, A. P. Vassilopoulos, and T. Keller, "Effect of thermal lag on glass transition temperature of polymers measured by DMA," *International Journal of Adhesion and Adhesives*, vol. 52, pp. 31–39, 2014.